INTERNATIONAL JOURNAL OF
NUMERICAL ANALYSIS AND MODELING
Volume 20, Number 4, Pages 577–595

doi: 10.4208/ijnam2023-1025

A SPLITTING SPECTRAL METHOD FOR THE NONLINEAR DIRAC-POISSON EQUATIONS

DANDAN WANG, YONG ZHANG, AND HANQUAN WANG*

Abstract. We develop a splitting spectral method for the time-dependent nonlinear Dirac-Poisson (DP) equations. Through time splitting method, we split the time-dependent nonlinear DP equations into linear and nonlinear subproblems. To advance DP from time t_n to t_{n+1}, the nonlinear subproblem can be integrated analytically, and linear Dirac and Poisson equation are well resolved by Fourier and Sine spectral method respectively. Compared with conventional numerical methods, our method achieves spectral accuracy in space, conserves total charge on the discrete level. Extensive numerical results confirm the spatial spectral accuracy, the second order temporal accuracy, and the l^2-stable property. Finally, an application from laser field is proposed to simulate the spin-flip phenomenon.

Key words. Nonlinear Dirac-Poisson equations, spectral method, splitting method, laser field, spin-flip.

1. Introduction

Maxwell-Dirac (MD) system represents the time-evolution of fast (relativistic) electrons and positrons within external and self-consistent generated electromagnetic fields, and it plays an important role in quantum electrodynamics [20, 21]. The system combining Maxwell equations and Dirac equations is of great significance to the progress of science and technology, the rapid development of information age. And it has been widely employed in many areas such as quantum cosmology, atomic physics, nuclear physics, gravitational physics [10, 23, 26].

Under the electrostatic condition, the Dirac-Poisson (DP) system can be directly derived from the MD system and it also can be adopted to study theoretically the structures and/or dynamical properties of materials. In 1966, Wakano obtained the localized solutions of the MD system under the electrostatic field [27]; in 1976, Chadam and Glassey studied the solution of the 2d MD system with zero magnetic field [9]; in 1994, Esteban and Sere confirmed the existence of stationary solutions for the DP system [13]; in 2014, Brinkman, Heitzinger and Markowich used the DP system to simulate graphene [7]; in 2017, Zhang et al. used variational methods to analyze the existence of infinitely many stationary solutions for the DP system [31].

Up to now, there are a few numerical methods to solve nonlinear Dirac equations: Finite difference methods [7, 17, 24], Runge-Kutta discontinuous Galerkin methods[25, 29, 30], Fourier spectral methods [1, 3, 4, 6, 16], while efficient high-order numerical methods for nonlinear DP equations are scarce.

In this paper, we propose a novel splitting spectral method for the time-dependent DP equations. In time, we apply the splitting method. In space, we apply Fourier spectral method and Sine spectral method to discretize the Dirac and Poisson equations, respectively. The merits of the proposed method for the nonlinear DP equations are that it is unconditionally stable, fast in computation,

Received by the editors on September 7, 2022 and, accepted on March 7, 2023.
2000 *Mathematics Subject Classification.* 65M70, 65M12, 81-08.
*Corresponding author.

has spectral accuracy in space, and conserves the particle number, momentum and energy of the system.

The organization of the article is following. In section 2, we introduce the nonlinear DP equations and its dimensionless formulation. Besides, we give the definition of charge, momentum, energy and prove the conservation laws. In section 3, we propose a splitting spectral method for the time-dependent DP equations and introduce the detailed numerical algorithm in time and space, respectively. In section 4, we analyze the stability and convergence of the splitting spectral method. In section 5, we present numerical tests in 1-d, 2-d and 3-d DP equations, respectively. As an application, we consider the laser-atom dynamics with the 2-d DP equations. Finally, conclusion is drawn.

2. The nonlinear DP equations

2.1. Introduction of the nonlinear DP equations. MD system has been studied widely in quantum electrodynamics, and in this paper, we consider the following electrostatic MD equations

$$i\hbar\partial_t \boldsymbol{\Psi} = (-i\hbar c\boldsymbol{\alpha}\cdot\boldsymbol{\nabla} + e\boldsymbol{\alpha}\cdot\boldsymbol{A} + mc^2\boldsymbol{\beta})\boldsymbol{\Psi} - e\phi\boldsymbol{\Psi}, \tag{1}$$

$$-\boldsymbol{\nabla}^2\phi = |e||\boldsymbol{\Psi}|^2. \tag{2}$$

In [12, 18], the equations are called Dirac-Poisson equations. And c is the speed of light, e is the elementary charge, m is the electron or positron mass, $\hbar$ is the Planck's constant, i is the imaginary unit, $\boldsymbol{A}(\boldsymbol{x},t) = (A_1(\boldsymbol{x},t), A_2(\boldsymbol{x},t), A_3(\boldsymbol{x},t))^T$ are the electromagnetic vector potentials, $\phi(\boldsymbol{x},t)$ is the electric potential. And the unknown $\boldsymbol{\Psi}$ is the 4-vector complex wave function of the 'spinorfield': $\boldsymbol{\Psi}(\boldsymbol{x},t) = (\Psi_1(\boldsymbol{x},t), \Psi_2(\boldsymbol{x},t), \Psi_3(\boldsymbol{x},t), \Psi_4(\boldsymbol{x},t))^T$, $\boldsymbol{x} = (x_1, x_2, x_3)^T$ is the spatial coordinates, $\boldsymbol{\nabla} = (\partial_1, \partial_2, \partial_3)^T$, and $\boldsymbol{\nabla}^2 = \partial_{11}^2 + \partial_{22}^2 + \partial_{33}^2$. Explicitly, $\boldsymbol{\alpha} = (\boldsymbol{\alpha}_1, \boldsymbol{\alpha}_2, \boldsymbol{\alpha}_3)^T$ and $\boldsymbol{\beta}$ are the 4×4 Pauli-Dirac matrices

$$\boldsymbol{\beta} = \begin{pmatrix} \boldsymbol{I} & \boldsymbol{0} \\ \boldsymbol{0} & -\boldsymbol{I} \end{pmatrix}, \quad \boldsymbol{\alpha}_\eta = \begin{pmatrix} \boldsymbol{0} & \boldsymbol{\sigma}_\eta \\ \boldsymbol{\sigma}_\eta & \boldsymbol{0} \end{pmatrix}, \quad \eta = 1,2,3,$$

where $\boldsymbol{I}, \boldsymbol{0}$ and $\boldsymbol{\sigma}_\eta (\eta = 1,2,3)$ are the 2×2 identity matrix, null matrix and Pauli matrices, respectively. i.e.

$$\boldsymbol{\sigma}_1 = \begin{pmatrix} 0 & 1 \\ 1 & 0 \end{pmatrix}, \quad \boldsymbol{\sigma}_2 = \begin{pmatrix} 0 & -i \\ i & 0 \end{pmatrix}, \quad \boldsymbol{\sigma}_3 = \begin{pmatrix} 1 & 0 \\ 0 & -1 \end{pmatrix}.$$

Multiplying both-hand sides of the Eq.(1) by $\frac{-i}{mc^2}$ to quantify it, we have

$$\frac{\hbar}{mc^2}\partial_t\boldsymbol{\Psi} = (-\frac{\hbar}{mc}\boldsymbol{\alpha}\cdot\boldsymbol{\nabla} - \frac{e}{mc^2}i\boldsymbol{\alpha}\cdot\boldsymbol{A} - i\boldsymbol{\beta})\boldsymbol{\Psi} + \frac{e}{mc^2}i\phi\boldsymbol{\Psi}. \tag{3}$$

Now, we rescale the space, the time, the wave function and the potential function by setting

$$\begin{gathered} t = \tfrac{\hbar}{mc^2}\tilde{t}, \quad \boldsymbol{x} = \tfrac{\hbar}{mc}\tilde{\boldsymbol{x}}, \quad \boldsymbol{A} = \tfrac{e}{mc^2}\tilde{\boldsymbol{A}}, \quad \phi = \tfrac{e}{mc^2}\tilde{\phi}, \\ \boldsymbol{\Psi} = (\tfrac{\hbar}{mc})^{3/2}\tilde{\boldsymbol{\Psi}}, \quad \tilde{\boldsymbol{\Psi}} = \tilde{\boldsymbol{\Psi}}(\tilde{\boldsymbol{x}},\tilde{t}), \quad \tilde{\boldsymbol{x}} \in \mathbb{R}^3. \end{gathered} \tag{4}$$

Substituting Eq.(4) into Eq.(3) and Eq.(2), then moving all $\sim$, we get the following dimensionless DP equations in 3-d

$$\begin{gathered} \partial_t\boldsymbol{\Psi} = (-\boldsymbol{\alpha}\cdot\boldsymbol{\nabla} - i\boldsymbol{\alpha}\cdot\boldsymbol{A} - i\boldsymbol{\beta})\boldsymbol{\Psi} + i\phi\boldsymbol{\Psi}, \\ \boldsymbol{\nabla}^2\phi = -\lambda^2|\boldsymbol{\Psi}|^2. \end{gathered} \tag{5}$$

where the coefficient of the Poisson equation depends on λ^2 which is related to the scaling value for wave function $\boldsymbol{\Psi}$.

Similarly to the dimension reduction of the nonlinear Schrödinger equation and/or the Schrödinger-Poisson equations with/without anisotropic external potentials[2], when the initial data $\boldsymbol{\Psi}(\boldsymbol{x},0)$ and the electromagneticpotentials $\phi(\boldsymbol{x},t)$ and $\boldsymbol{A}(\boldsymbol{x},t)$ are strongly confined in the x_3-direction and thus $\boldsymbol{\Psi}$ is formally assumed to be concentrated on the x_1x_2-plane, then the 3-d DP equations (5) can be reduced to the 2-d DP equations with $\boldsymbol{x} = (x_1, x_2)^T \in \mathbb{R}^2$. When $\Psi_4 = \Psi_3$, $\Psi_2 = \Psi_1$ and the proper assumptions on the initial data and the external electromagnetic potential, the 3-d DP equations (5) can be reduced to the 1-d DP equations in the x_1-direction. Therefore, the DP equations in 3-d (5), in 2-d and in 1-d can be written in a unified way in d-dimensions ($d = 1, 2, 3$)

$$\begin{aligned} \partial_t \boldsymbol{\Psi} &= (-\textstyle\sum_{\eta=1}^{d} \boldsymbol{\alpha}_\eta \partial_\eta - i \sum_{\eta=1}^{d} \boldsymbol{\alpha}_\eta A_\eta - i\boldsymbol{\beta})\boldsymbol{\Psi} + i\phi\boldsymbol{\Psi}, \\ \boldsymbol{\nabla}^2\phi &= -\lambda^2 |\boldsymbol{\Psi}|^2. \end{aligned} \tag{6}$$

2.2. Conservation laws of the nonlinear DP equations. When potentials $\boldsymbol{A}$ are time-independent, we prove that the charge, the momentum and the energy of particle are conserved in the DP equations (6).

The charge $\mathcal{Q}$ is

$$\mathcal{Q}(t) = \int_{\mathbb{R}^d} \bar{\boldsymbol{\Psi}}^T \boldsymbol{\Psi} \, d\boldsymbol{x}. \tag{7}$$

The momentum $\mathbf{P}$ is

$$\mathcal{P}_\eta(t) = \int_{\mathbb{R}^d} \mathrm{Im}(\partial_\eta \bar{\boldsymbol{\Psi}}^T \boldsymbol{\Psi}) \, d\boldsymbol{x}. \quad (\eta = 1, \ldots, d) \tag{8}$$

The total energy $\mathcal{E}$ is

$$\begin{aligned} \mathcal{E}(t) = \int_{\mathbb{R}^d} -\mathrm{Im}(\sum_{\eta=1}^{d} \bar{\boldsymbol{\Psi}}^T \boldsymbol{\alpha}_\eta \, \partial_\eta \boldsymbol{\Psi}) - \bar{\boldsymbol{\Psi}}^T \boldsymbol{\beta} \boldsymbol{\Psi} \, d\boldsymbol{x} + \int_{\mathbb{R}^d} \phi \bar{\boldsymbol{\Psi}}^T \boldsymbol{\Psi} \\ - \sum_{\eta=1}^{d} A_\eta \bar{\boldsymbol{\Psi}}^T \boldsymbol{\alpha}_\eta \boldsymbol{\Psi} \, d\boldsymbol{x} + \int_{\mathbb{R}^d} \frac{1}{2} |\boldsymbol{\nabla}\phi|^2 \, d\boldsymbol{x}, \end{aligned} \tag{9}$$

where Fermion energy $\mathcal{E}_{\boldsymbol{\Psi}} = \int_{\mathbb{R}^d} -\mathrm{Im}(\sum_{\eta=1}^{d} \bar{\boldsymbol{\Psi}}^T \boldsymbol{\alpha}_\eta \, \partial_\eta \boldsymbol{\Psi}) - \bar{\boldsymbol{\Psi}}^T \boldsymbol{\beta} \boldsymbol{\Psi} \, d\boldsymbol{x}$, interaction energy $\mathcal{E}_I = \int_{\mathbb{R}^d} \phi \bar{\boldsymbol{\Psi}}^T \boldsymbol{\Psi} - \sum_{\eta=1}^{d} A_\eta \bar{\boldsymbol{\Psi}}^T \boldsymbol{\alpha}_\eta \boldsymbol{\Psi} \, d\boldsymbol{x}$ and electromagnetic energy $\mathcal{E}_{em} = \int_{\mathbb{R}^d} \frac{1}{2} |\boldsymbol{\nabla}\phi|^2 \, d\boldsymbol{x}$.

Among Eqs.(7)-(9), $\mathrm{Im}(\boldsymbol{\Psi})$ denotes the imaginary part of the complex quantity $\boldsymbol{\Psi}$, $\bar{\boldsymbol{\Psi}}$ is the conjugate of the complex quantity $\boldsymbol{\Psi}$.

Proposition 2.1. *If the solution $\boldsymbol{\Psi}$ and ϕ satisfy*

$$\lim_{|\boldsymbol{x}|\to+\infty} |\boldsymbol{\Psi}(\boldsymbol{x},t)| = \mathbf{0}, \qquad \lim_{|\boldsymbol{x}|\to+\infty} |\partial_{\boldsymbol{x}} \boldsymbol{\Psi}(\boldsymbol{x},t)| = \mathbf{0},$$

and

$$\lim_{|\boldsymbol{x}|\to+\infty} |\phi(\boldsymbol{x},t)| = 0, \qquad \lim_{|\boldsymbol{x}|\to+\infty} |\partial_{\boldsymbol{x}} \phi(\boldsymbol{x},t)| = 0,$$

uniformly for $t \in \mathbb{R}$, then

$$\frac{d}{dt}\mathcal{Q}(t) = 0, \quad \frac{d}{dt}\mathbf{P}(t) = \mathbf{0}, \quad \textit{and} \quad \frac{d}{dt}\mathcal{E}(t) = 0.$$

Proof. We first give the proof in 1-d. In 1-d, we take $\Psi_4 = \Psi_3$, $\Psi_2 = \Psi_1$, we get the following 1-d DP equations

$$\begin{aligned} \partial_t \Psi_1 &= -\partial_1 \Psi_2 - iA_1 \Psi_2 - i\Psi_1 + i\phi\Psi_1, \\ \partial_t \Psi_2 &= -\partial_1 \Psi_1 - iA_1 \Psi_1 + i\Psi_2 + i\phi\Psi_2. \end{aligned} \tag{10}$$

Taking the conjugate of both-hand sides of Eq.(10), we obtain

$$\begin{aligned}\partial_t\bar{\Psi}_1 &= -\partial_1\bar{\Psi}_2 + iA_1\bar{\Psi}_2 + i\bar{\Psi}_1 - i\phi\bar{\Psi}_1,\\ \partial_t\bar{\Psi}_2 &= -\partial_1\bar{\Psi}_1 + iA_1\bar{\Psi}_1 - i\bar{\Psi}_2 - i\phi\bar{\Psi}_2.\end{aligned} \tag{11}$$

(1) Proof of $\frac{d}{dt}\mathcal{Q}(t) = 0$. Multiplying both-hand sides of Eqs.(10) and (11) by $\bar{\Psi}_1, \bar{\Psi}_2$ and Ψ_1, Ψ_2, respectively, then plugging the results into the following equation and one finds

$$\begin{aligned}&\frac{d}{dt}\mathcal{Q}(t)\\ &= \frac{d}{dt}\int_{\mathbb{R}}(|\Psi_1|^2 + |\Psi_2|^2)\ dx_1 = \int_{\mathbb{R}}(\partial_t\bar{\Psi}_1\Psi_1 + \partial_t\Psi_1\bar{\Psi}_1 + \partial_t\bar{\Psi}_2\Psi_2 + \partial_t\Psi_2\bar{\Psi}_2)\ dx_1\\ &= \int_{\mathbb{R}} -\partial_1(\bar{\Psi}_2\Psi_1 + \bar{\Psi}_1\Psi_2)\ dx_1 = 0.\end{aligned}$$

(2) Proof of $\frac{d}{dt}\mathcal{P}(t) = 0$.

Multiplying both-hand sides of Eqs.(10) and (11) by $\partial_1\bar{\Psi}_1, \partial_1\bar{\Psi}_2$ and $\partial_1\Psi_1$, $\partial_1\Psi_2$, respectively, then plugging the results into the following equation and one gets

$$\begin{aligned}&\frac{d}{dt}\mathcal{P}(t)\\ &= \frac{d}{dt}\int_{\mathbb{R}} Im(\partial_1\bar{\Psi}_1\Psi_1 + \partial_1\bar{\Psi}_2\Psi_2)\ dx_1\\ &= \int_{\mathbb{R}} Im(-\partial_1\Psi_1\partial_t\bar{\Psi}_1 + \partial_1\bar{\Psi}_1\partial_t\Psi_1 - \partial_1\Psi_2\partial_t\bar{\Psi}_2 + \partial_1\bar{\Psi}_2\partial_t\Psi_2)\ dx_1\\ &= \int_{\mathbb{R}} Im[-iA_1\partial_1(\bar{\Psi}_2\Psi_1 + \bar{\Psi}_1\Psi_2) - i\partial_1(|\Psi_1|^2 + |\Psi_2|^2) + i\phi\partial_1(|\Psi_1|^2 + |\Psi_2|^2)]\ dx_1\\ &= 0.\end{aligned}$$

Here integration by parts has been used, i.e.

$$\int_{\mathbb{R}} \Psi\partial_x(\partial_t\bar{\Psi})\ dx = \Psi\,\partial_t\bar{\Psi}|_{\mathbb{R}} - \int_{\mathbb{R}} \partial_x\Psi\,\partial_t\bar{\Psi}\ dx.$$

(3) Proof of $\frac{d}{dt}\mathcal{E}(t) = 0$. The following process is based on the result of **(1)**, conditions of Proposition 2.1 and the method of integration by parts.

- Multiplying both-hand sides of Eqs.(10) and (11) by $\partial_1\bar{\Psi}_2, \partial_1\bar{\Psi}_1$ and $\partial_1\Psi_2$, $\partial_1\Psi_1$, respectively, then one reaches

$$\begin{aligned}\frac{d}{dt}\mathcal{E}_{\mathbf{\Psi}}(t) &= \frac{d}{dt}\int_{\mathbb{R}}[-Im(\bar{\Psi}_2\partial_1\Psi_1 + \bar{\Psi}_1\partial_1\Psi_2) - (|\Psi_1|^2 - |\Psi_2|^2)]\ dx_1\\ &= \int_{\mathbb{R}} Im[i\phi\partial_1(\bar{\Psi}_2\Psi_1 + \bar{\Psi}_1\Psi_2)] - 2A_1 i(\bar{\Psi}_2\Psi_1 - \bar{\Psi}_1\Psi_2)\ dx_1\end{aligned}$$

- Multiplying both-hand sides of Eqs.(10) and (11) by $\bar{\Psi}_2, \bar{\Psi}_1$ and Ψ_2, Ψ_1, respectively, then one gets

$$\begin{aligned}\frac{d}{dt}\mathcal{E}_I(t) &= \frac{d}{dt}\int_{\mathbb{R}} \phi(|\Psi_1|^2 + |\Psi_2|^2) - A_1(\bar{\Psi}_2\Psi_1 + \bar{\Psi}_1\Psi_2)\ dx_1\\ &= \int_{\mathbb{R}} -\phi\partial_1(\bar{\Psi}_2\Psi_1 + \bar{\Psi}_1\Psi_2) + 2A_1 i(\bar{\Psi}_2\Psi_1 - \bar{\Psi}_1\Psi_2)\ dx_1\end{aligned}$$

- Obviously,

$$\frac{d}{dt}\mathcal{E}_{em}(t) = \frac{d}{dt}\int_{\mathbb{R}}\frac{1}{2}|\partial_1\phi|^2\ dx_1 = 0.$$

Finally,

$$\frac{d}{dt}\mathcal{E}(t) = \frac{d}{dt}\mathcal{E}_\Psi(t) + \frac{d}{dt}\mathcal{E}_I(t) + \frac{d}{dt}\mathcal{E}_{em}(t) = 0.$$

Similar proof can be derived for the problem in 2-d and 3-d. For simplicity, we omit the details here. □

In addition, we find that the following conservation law holds

$$\partial_t \rho(\boldsymbol{x},t) + \boldsymbol{\nabla}\cdot\boldsymbol{J}(\boldsymbol{x},t) = 0, \quad t \geq 0, \quad \boldsymbol{x}\in\mathbb{R}^d, \tag{12}$$

here particle density $\rho = \bar{\boldsymbol{\Psi}}^T\boldsymbol{\Psi}$, current density $\boldsymbol{J} = \bar{\boldsymbol{\Psi}}^T\boldsymbol{\alpha}\boldsymbol{\Psi}$.

3. A splitting spectral method

In this section, we present a splitting spectral method for the DP equations (6). In numerical computation, we truncate the problem into the following initial-boundary value problem

$$\partial_t\boldsymbol{\Psi} = (-\sum_{\eta=1}^{d}\boldsymbol{\alpha}_\eta\partial_\eta - i\sum_{\eta=1}^{d}\boldsymbol{\alpha}_\eta A_\eta(\boldsymbol{x},t))\boldsymbol{\Psi} - i(\boldsymbol{\beta}-\phi(\boldsymbol{x},t)\,\boldsymbol{I})\boldsymbol{\Psi},\ \boldsymbol{x}\in\Omega,\ t\geq 0 \tag{13}$$

$$\boldsymbol{\nabla}^2\phi(\boldsymbol{x},t) = -\lambda^2|\boldsymbol{\Psi}(\boldsymbol{x},t)|^2, \quad \boldsymbol{x}\in\Omega, \quad t\geq 0 \tag{14}$$

$$\boldsymbol{\Psi}(\boldsymbol{x},t)\ \textit{is periodic, and}\ \phi(\boldsymbol{x},t) = 0, \quad \boldsymbol{x}\in\partial\Omega, \quad t\geq 0, \tag{15}$$

$$\boldsymbol{\Psi}(\boldsymbol{x},t) = \boldsymbol{\Psi}_0(\boldsymbol{x}), \quad \boldsymbol{x}\in\Omega. \tag{16}$$

where $\Omega = (a,b)$ in one dimension, $\Omega = (a_1,b_1)\times(a_2,b_2)$ in two dimension and $\Omega = (a_1,b_1)\times(a_2,b_2)\times(a_3,b_3)$ in three dimension. $\partial\Omega$ is the boundary of Ω, $\boldsymbol{\Psi}_0(\boldsymbol{x})$ is a known function.

We choose the spatial mesh size $h_\eta = \frac{b_\eta - a_\eta}{M_\eta}(\eta = 1,\cdots,d)$ in the x_η-direction with M_η given integer and the time step Δt, respectively. We denote the spatial grid points as

$$\boldsymbol{x}_{\boldsymbol{p}} = (x_{1p_1},\cdots,x_{dp_d})^T,\ \ \boldsymbol{p} = (p_1,\cdots,p_d)^T\ \ \textit{and}\ \ \boldsymbol{p}\in\mathcal{N},\ \ \boldsymbol{h} = (h_1,\cdots,h_d)^T,\ \ d = 1,2,3,$$

where

$$\mathcal{N} = \{\boldsymbol{p}|0\leq p_1\leq M_1,\cdots,0\leq p_d\leq M_d\},$$
$$x_{1p_1} = a_1 + p_1h_1,\cdots,x_{dp_d} = a_d + p_dh_d$$

and temporal grids as

$$t_n = n\Delta t, \quad n = 0,1,2,\cdots.$$

3.1. Splitting method in time. Two splitting methods are proposed here for the DP equations (13)-(14). First, from time $t = t_n$ to $t = t_{n+1}$, it may be solved as the following two steps

$$\partial_t\boldsymbol{\Psi}(\boldsymbol{x},t) = -i(\boldsymbol{\beta}-\phi(\boldsymbol{x},t)\,\boldsymbol{I} + \sum_{\eta=1}^{d}\boldsymbol{\alpha}_\eta A_\eta(\boldsymbol{x},t))\boldsymbol{\Psi}(\boldsymbol{x},t) = \mathcal{A}\boldsymbol{\Psi}(\boldsymbol{x},t), \tag{17}$$
$$\boldsymbol{\nabla}^2\phi(\boldsymbol{x},t) = -\lambda^2|\boldsymbol{\Psi}(\boldsymbol{x},t)|^2, \qquad t\in[t_n,t_{n+1}]$$

$$\partial_t\boldsymbol{\Psi}(\boldsymbol{x},t) = -\sum_{\eta=1}^{d}\boldsymbol{\alpha}_\eta\partial_\eta\boldsymbol{\Psi}(\boldsymbol{x},t) = \mathcal{B}\boldsymbol{\Psi}(\boldsymbol{x},t), \qquad t\in[t_n,t_{n+1}]. \tag{18}$$

Therefore, the Eqs.(13)-(14) are solved in the following way

$$\boldsymbol{\Psi}(\boldsymbol{x},t+\Delta t)\approx e^{\mathcal{A}\Delta t}e^{\mathcal{B}\Delta t}\boldsymbol{\Psi}(\boldsymbol{x},t). \tag{19}$$

For the nonlinear part Eq.(17), when the electromagnetic potentials $\boldsymbol{A}$ are time-dependent, we split it into two sub-flows, i.e.,

$$\partial_t \boldsymbol{\Psi}(\boldsymbol{x},t) = -i(\boldsymbol{\beta} - \phi(\boldsymbol{x},t)\,\boldsymbol{I})\boldsymbol{\Psi}(\boldsymbol{x},t) = \mathcal{A}_1\boldsymbol{\Psi}(\boldsymbol{x},t),$$

$$\boldsymbol{\nabla}^2\phi(\boldsymbol{x},t) = -\lambda^2|\boldsymbol{\Psi}(\boldsymbol{x},t)|^2, \qquad t\in[t_n,t_{n+1}] \tag{20a}$$

$$\partial_t \boldsymbol{\Psi}(\boldsymbol{x},t) = -i\sum_{\eta=1}^{d}\boldsymbol{\alpha}_\eta A_\eta(\boldsymbol{x},t)\boldsymbol{\Psi}(\boldsymbol{x},t) = \mathcal{A}_2\boldsymbol{\Psi}(\boldsymbol{x},t), \qquad t\in[t_n,t_{n+1}] \tag{20b}$$

or symbolically we will let $e^{\mathcal{A}\Delta t}\approx e^{\mathcal{A}_1\Delta t}e^{\mathcal{A}_2\Delta t}$ in Eq. (19) since $\mathcal{A}=\mathcal{A}_1+\mathcal{A}_2$.

In the first flow (20a), multiplying the conjugate of Eq.(20a) with multiplying $\boldsymbol{\Psi}$, and then subtracting that from the result that multiplying both-hand sides of the Eq.(20a) by $\bar{\boldsymbol{\Psi}}$, we have $\frac{d}{dt}|\boldsymbol{\Psi}(\boldsymbol{x},t)|^2=0$. Namely,

$$|\boldsymbol{\Psi}(\boldsymbol{x},t)|^2 = |\boldsymbol{\Psi}(\boldsymbol{x},t_n)|^2, \quad t\in[t_n,t_{n+1}]. \tag{21}$$

Then, we obtain the exact solution to Eq.(20a)

$$\boldsymbol{\Psi}(\boldsymbol{x},t) = e^{-i(t-t_n)(\beta-\phi(\boldsymbol{x},t_n)\,\boldsymbol{I})}\boldsymbol{\Psi}(\boldsymbol{x},t_n), \quad t\in[t_n,t_{n+1}], \tag{22}$$

where the solution $\phi(\boldsymbol{x},t_n)$ is obtained from the following Poisson equation

$$\boldsymbol{\nabla}^2\phi(\boldsymbol{x},t) = -\lambda^2|\boldsymbol{\Psi}(\boldsymbol{x},t_n)|^2, \quad t\in[t_n,t_{n+1}]. \tag{23}$$

In the second flow (20b), we treat the electromagnetic potentials $\boldsymbol{A}(\boldsymbol{x},t)$ at time $t=t_n$ explicitly and denser time grid points chosen to avoid its impact on accuracy. Therefore, we have the exact integration

$$\boldsymbol{\Psi}(\boldsymbol{x},t) = e^{-i(t-t_n)\sum_{\eta=1}^{d}\boldsymbol{\alpha}_\eta A_\eta(\boldsymbol{x},t_n)}\,\boldsymbol{\Psi}(\boldsymbol{x},t_n), \quad t\in[t_n,t_{n+1}]. \tag{24}$$

The linear part Eq.(18) can be solved with Fourier spectral method. In this step, we need to apply the technique of matrix diagonalization.

Next, we apply Strang splitting method[5, 11, 14, 28] for the Dirac equations (13) from time $t=t_n$ to $t=t_{n+1}$

$$\partial_t\boldsymbol{\Psi}^{(1)}(\boldsymbol{x},t) = \mathcal{B}\boldsymbol{\Psi}^{(1)}(\boldsymbol{x},t), \quad \boldsymbol{\Psi}^{(1)}(\boldsymbol{x},t_n) = \boldsymbol{\Psi}^{(1)}(\boldsymbol{x},t_n), \qquad t\in[t_n,t_{n+\frac{1}{2}}]$$

$$\partial_t\boldsymbol{\Psi}^{(2)}(\boldsymbol{x},t) = \mathcal{A}\boldsymbol{\Psi}^{(2)}(\boldsymbol{x},t), \quad \boldsymbol{\Psi}^{(2)}(\boldsymbol{x},t_n) = \boldsymbol{\Psi}^{(1)}(\boldsymbol{x},t_{n+\frac{1}{2}}), \qquad t\in[t_n,t_{n+1}]$$

$$\partial_t\boldsymbol{\Psi}^{(3)}(\boldsymbol{x},t) = \mathcal{B}\boldsymbol{\Psi}^{(3)}(\boldsymbol{x},t), \quad \boldsymbol{\Psi}^{(3)}(\boldsymbol{x},t_{n+\frac{1}{2}}) = \boldsymbol{\Psi}^{(2)}(\boldsymbol{x},t_{n+1}), \quad t\in[t_{n+\frac{1}{2}},t_{n+1}].$$

Therefore, the Eq.(13) is solved in the following way

$$\boldsymbol{\Psi}(\boldsymbol{x},t+\Delta t)\approx e^{\mathcal{B}\Delta t/2}e^{\mathcal{A}\Delta t}e^{\mathcal{B}\Delta t/2}\boldsymbol{\Psi}(\boldsymbol{x},t). \tag{25}$$

Here the time increments are $\Delta t/2$ for the linear operator $\mathcal{B}$, Δt for the nonlinear operator $\mathcal{A}$. This kind of splitting method induces an error of $O(\Delta t^3)$, and can be improved to arbitrary order at the cost of more computation time.

3.2. Spectral method in d-dimensional space. In this section, we present how to apply the spectral method to solve the Dirac equations and Poisson equation in different dimensioms. By the dimension reduction, we can easily solve two-dimensional and one-dimensional problems. If we apply Fourier spectral method to the Poisson equation, it does not have a well defined limit for $\boldsymbol{x}\to\boldsymbol{0}$ and it will affect the overall numerical accuracy. In order to get better numerical accuracy, we use Sine spectral method to solve Poisson equation and Fourier spectral method to discretize Dirac equations, respectively. For convenience, performing the following symbolic approximation

$$\boldsymbol{\Psi}_{\boldsymbol{p}}^n \approx \boldsymbol{\Psi}(\boldsymbol{x}_{\boldsymbol{p}},t_n), \quad \phi_{\boldsymbol{p}}^n \approx \phi(\boldsymbol{x}_{\boldsymbol{p}},t_n), \quad \boldsymbol{p}=(p_1,\cdots,p_d)^T, \quad d=1,2,3, \tag{26}$$

and $\mathbf{\Psi}^n, \phi^n$ is the solution vector at time $t = t_n$ with components $\mathbf{\Psi}^n_{\boldsymbol{p}}, \phi^n_{\boldsymbol{p}}$.

From time $t = t_n$ to $t = t_{n+1}$, we discretize the DP equations (13)-(14) as follows

(1) For the Poisson equation (14), we can construct the following Sine expansion for an unknown function $\phi(\boldsymbol{x}, t)$ with zero boundaries defined on Ω

$$\phi(\boldsymbol{x}, t) \approx \sum_{\boldsymbol{j}\in\mathcal{H}} \hat{\phi}_{\boldsymbol{j}}(t) sin(\boldsymbol{\mu_j} \cdot (\boldsymbol{x} - \boldsymbol{a})), \quad t \in [t_n, t_{n+1}] \tag{27}$$

where $\boldsymbol{a} = (a_1, \cdots, a_d)^T$, $\boldsymbol{j} = (j_1, \cdots, j_d)^T$, $\boldsymbol{M} = (M_1, \cdots, M_d)^T$,

$$\hat{\phi}_{\boldsymbol{j}} \approx \frac{2^d}{M_1 \cdots M_d} \sum_{\boldsymbol{p}\in\mathcal{H}} \phi_{\boldsymbol{p}}\, sin(\boldsymbol{\mu_j}(\boldsymbol{x_p} - \boldsymbol{a})), \quad \boldsymbol{j} \in \mathcal{H}$$

and

$$\mathcal{H} = \{\boldsymbol{j} | 1 \le j_1 \le M_1 - 1, \cdots, 1 \le j_d \le M_d - 1\},$$
$$\boldsymbol{\mu_j} = (\mu_{j_1}, \cdots, \mu_{j_d})^T = (\frac{\pi j_1}{b_1 - a_1}, \cdots, \frac{\pi j_d}{b_d - a_d})^T, \quad \boldsymbol{j} \in \mathcal{H}.$$

Substituting Eq.(27) into Eq.(14) and applying the orthogonality of the Sine series, we get the following ODE

$$|\boldsymbol{\mu_j}|^2\, \hat{\phi}_{\boldsymbol{j}}(t) = \lambda^2\, \hat{\rho}_{\boldsymbol{j}}(t) = \lambda^2\, (\widehat{|\mathbf{\Psi}_{\boldsymbol{j}}(t)|^2}), \quad t \in [t_n, t_{n+1}] \tag{28}$$

namely,

$$\hat{\phi}_{\boldsymbol{j}}(t) = \lambda^2\, \hat{\rho}_{\boldsymbol{j}}(t) / |\boldsymbol{\mu_j}|^2.$$

Finally, we obtain the numerical solution of Eq.(14) is that $\phi^{n+1}_{\boldsymbol{p}}$.

(2) For the electromagnetic potential flow (20b), the Pauli-Dirac matrices $\boldsymbol{\alpha}_\eta$ are unitary, and the term

$$\sum_{\eta=1}^{d} \boldsymbol{\alpha}_\eta A_\eta(\boldsymbol{x_j}, t_n) = \boldsymbol{P}^n_{\boldsymbol{j}}\, \boldsymbol{\Lambda}^n_{\boldsymbol{j}}\, (\boldsymbol{P}^n_{\boldsymbol{j}})^{-1}, \quad \boldsymbol{j} \in \mathcal{N}, \tag{29}$$

where $\boldsymbol{\Lambda}^n_{\boldsymbol{j}} = \boldsymbol{\Lambda}(\boldsymbol{x_j}, t_n)$ is a diagonal matrix and $\boldsymbol{P}^n_{\boldsymbol{j}} = \boldsymbol{P}(\boldsymbol{x_j}, t_n)$ is a complex orthogonormal matrix, i.e. $\bar{\boldsymbol{P}^n_{\boldsymbol{j}}}^T = (\boldsymbol{P}^n_{\boldsymbol{j}})^{-1}$. Then we get one ODE

$$\partial_t \mathbf{\Psi} = -i\, \boldsymbol{P}^n_{\boldsymbol{j}}\, \boldsymbol{\Lambda}^n_{\boldsymbol{j}}\, (\boldsymbol{P}^n_{\boldsymbol{j}})^{-1}\, \mathbf{\Psi}. \tag{30}$$

Finally, we get the solution at time $t = t_{n+1}$

$$\mathbf{\Psi}(t_{n+1}) = \boldsymbol{P}^n_{\boldsymbol{j}}\, e^{-i\Delta t \boldsymbol{\Lambda}^n_{\boldsymbol{j}}}\, (\boldsymbol{P}^n_{\boldsymbol{j}})^{-1}\, \mathbf{\Psi}(t_n). \tag{31}$$

(3) For the linear part of Dirac equations (13), namely, Eq.(18), we can construct the following Fourier expansion for an unknown function $\mathbf{\Psi}(\boldsymbol{x}, t)$ with periodic boundaries defined on Ω

$$\mathbf{\Psi}(\boldsymbol{x}, t) \approx I_{\mathcal{M}}(\mathbf{\Psi}(\boldsymbol{x}, t)) = \sum_{\boldsymbol{j}\in\mathcal{M}} \hat{\mathbf{\Psi}}_{\boldsymbol{j}}(t) e^{i\boldsymbol{\mu_j}\cdot(\boldsymbol{x}-\boldsymbol{a})}, \quad t \in [t_n, t_{n+1}], \tag{32}$$

where

$$\hat{\mathbf{\Psi}}_{\boldsymbol{j}} = \frac{1}{M_1 \cdots M_d} \sum_{\boldsymbol{p}\in\mathcal{L}} \mathbf{\Psi}_{\boldsymbol{p}}\, e^{-i\boldsymbol{\mu_j}\cdot(\boldsymbol{x_p}-\boldsymbol{a})}, \quad \boldsymbol{j} \in \mathcal{M},$$
$$\mathcal{L} = \{\boldsymbol{p} | 0 \le p_1 \le M_1 - 1, \cdots, 0 \le p_d \le M_d - 1\}$$

and

$$\mathcal{M} = \{\boldsymbol{j} | -\frac{M_1}{2} \le j_1 \le \frac{M_1}{2}, \cdots, -\frac{M_d}{2} \le j_d \le \frac{M_d}{2}\},$$
$$\boldsymbol{\mu_j} = (\mu_{j_1}, \cdots, \mu_{j_d})^T = (\frac{2\pi j_1}{b_1 - a_1}, \cdots, \frac{2\pi j_d}{b_d - a_d})^T, \quad \boldsymbol{j} \in \mathcal{M}.$$

Substituting Eq.(32) into Eq.(18), integrate the result over $\boldsymbol{x} \in \Omega$, and then noticing the orthogonality of the Fourier series, we get the following ODEs

$$\partial_t \hat{\boldsymbol{\Psi}}_{\boldsymbol{j}} = \boldsymbol{D}\, \hat{\boldsymbol{\Psi}}_{\boldsymbol{j}}, \quad \boldsymbol{j} \in \mathcal{M}, \quad t \in [t_n, t_{n+1}]. \tag{33}$$

Since the unitary matrix is diagonalizable, i.e. there exist a diagonal matrix $\boldsymbol{\Lambda}$ and a complex orthogonormal matrix $\boldsymbol{P}$, i.e. $\bar{\boldsymbol{P}}^T = \boldsymbol{P}^{-1}$. And in 1d,

$$\boldsymbol{D} = -i \begin{pmatrix} 0 & \mu_{j_1} \\ \mu_{j_1} & 0 \end{pmatrix},$$

in 2d,

$$\boldsymbol{D} = -i[\boldsymbol{\alpha}_1 \mu_{j_1} + \boldsymbol{\alpha}_2 \mu_{j_2}],$$

in 3d,

$$\boldsymbol{D} = -i[\boldsymbol{\alpha}_1 \mu_{j_1} + \boldsymbol{\alpha}_2 \mu_{j_2} + \boldsymbol{\alpha}_3 \mu_{j_3}].$$

Therefore,

$$\boldsymbol{D} = \boldsymbol{P}\boldsymbol{\Lambda}\boldsymbol{P}^{-1}.$$

Setting $\hat{\boldsymbol{\Phi}}_{\boldsymbol{j}} = \boldsymbol{P}^{-1}\hat{\boldsymbol{\Psi}}_{\boldsymbol{j}}$, Eq.(33) is rewritten as

$$\partial_t \hat{\boldsymbol{\Phi}}_{\boldsymbol{j}} = \boldsymbol{\Lambda}\hat{\boldsymbol{\Phi}}_{\boldsymbol{j}}. \tag{34}$$

Solving Eq.(34), we can get

$$\hat{\boldsymbol{\Phi}}_{\boldsymbol{j}}(t_{n+1}) = e^{\boldsymbol{\Lambda}\Delta t}\, \hat{\boldsymbol{\Phi}}_{\boldsymbol{j}}(t_n), \ \textit{and}\ \hat{\boldsymbol{\Psi}}_{\boldsymbol{j}}(t_{n+1}) = \boldsymbol{P}\hat{\boldsymbol{\Phi}}_{\boldsymbol{j}}(t_{n+1}), \ \boldsymbol{j} \in \mathcal{M}. \tag{35}$$

Finally, we obtain the numerical solution of Eq.(18) is that $\boldsymbol{\Psi}_{\boldsymbol{p}}^{n+1}$.

From time $t = t_n$ to $t = t_{n+1}$, we evolve the following steps via the Sequential splitting

$$\hat{\phi}_{\boldsymbol{j}}^n = \lambda^2\, (\widehat{|\boldsymbol{\Psi}_{\boldsymbol{j}}^n|^2})/|\boldsymbol{\mu}_{\boldsymbol{j}}|^2 \tag{36}$$

$$\phi_{\boldsymbol{p}}^{n+1} = \sum_{\boldsymbol{j}\in\mathcal{H}} \hat{\phi}_{\boldsymbol{j}}^n\, sin(\boldsymbol{\mu}_{\boldsymbol{j}}(\boldsymbol{x}_{\boldsymbol{p}} - \boldsymbol{a})) \tag{37}$$

$$\boldsymbol{\Psi}_{\boldsymbol{p}}^* = e^{-i(\boldsymbol{\beta} - \phi_{\boldsymbol{p}}^{n+1}\boldsymbol{I})\Delta t}\, \boldsymbol{\Psi}_{\boldsymbol{p}}^n \tag{38}$$

$$\boldsymbol{\Psi}_{\boldsymbol{p}}^{**} = \boldsymbol{P}_{\boldsymbol{p}}^n\, e^{-i\Delta t \boldsymbol{\Lambda}_{\boldsymbol{p}}^n}\, (\boldsymbol{P}_{\boldsymbol{p}}^n)^{-1}\, \boldsymbol{\Psi}_{\boldsymbol{p}}^* \tag{39}$$

$$\boldsymbol{\Psi}_{\boldsymbol{p}}^{n+1} = \sum_{\boldsymbol{j}\in\mathcal{M}} \boldsymbol{P}\, e^{\boldsymbol{\Lambda}\Delta t}\, \boldsymbol{P}^{-1}\, \hat{\boldsymbol{\Psi}}_{\boldsymbol{j}}^{**}\, e^{i\boldsymbol{\mu}_{\boldsymbol{j}}\cdot(\boldsymbol{x}_{\boldsymbol{p}} - \boldsymbol{a})} \tag{40}$$

From time $t = t_n$ to $t = t_{n+1}$, we iterate the following steps via the Strang splitting

$$\hat{\phi}_{\boldsymbol{j}}^n = \lambda^2\, (\widehat{|\boldsymbol{\Psi}_{\boldsymbol{j}}^n|^2})/|\boldsymbol{\mu}_{\boldsymbol{j}}|^2 \tag{41}$$

$$\phi_{\boldsymbol{p}}^{n+1} = \sum_{\boldsymbol{j}\in\mathcal{H}} \hat{\phi}_{\boldsymbol{j}}^n\, sin(\boldsymbol{\mu}_{\boldsymbol{j}}(\boldsymbol{x}_{\boldsymbol{p}} - \boldsymbol{a})) \tag{42}$$

$$\boldsymbol{\Psi}_{\boldsymbol{p}}^* = \sum_{\boldsymbol{j}\in\mathcal{M}} \boldsymbol{P}\, e^{\boldsymbol{\Lambda}\Delta t/2}\, \boldsymbol{P}^{-1}\, \hat{\boldsymbol{\Psi}}_{\boldsymbol{j}}^n\, e^{i\boldsymbol{\mu}_{\boldsymbol{j}}\cdot(\boldsymbol{x}_{\boldsymbol{p}} - \boldsymbol{a})} \tag{43}$$

$$\boldsymbol{\Psi}_{\boldsymbol{p}}^{**} = e^{-i(\boldsymbol{\beta} - \phi_{\boldsymbol{p}}^{n+1}\boldsymbol{I})\Delta t}\, \boldsymbol{\Psi}_{\boldsymbol{p}}^* \tag{44}$$

$$\boldsymbol{\Psi}_{\boldsymbol{p}}^{***} = \boldsymbol{P}_{\boldsymbol{p}}^n\, e^{-i\Delta t \boldsymbol{\Lambda}_{\boldsymbol{p}}^n}\, (\boldsymbol{P}_{\boldsymbol{p}}^n)^{-1}\, \boldsymbol{\Psi}_{\boldsymbol{p}}^{**} \tag{45}$$

$$\boldsymbol{\Psi}_{\boldsymbol{p}}^{n+1} = \sum_{\boldsymbol{j}\in\mathcal{M}} \boldsymbol{P}\, e^{\boldsymbol{\Lambda}\Delta t/2}\, \boldsymbol{P}^{-1}\, \hat{\boldsymbol{\Psi}}_{\boldsymbol{j}}^{***}\, e^{i\boldsymbol{\mu}_{\boldsymbol{j}}\cdot(\boldsymbol{x}_{\boldsymbol{p}} - \boldsymbol{a})}. \tag{46}$$

4. Stability analysis and error estimates for the splitting spectral method

In the past section, we use two splitting techniques to discrete equation in time. Compared with the Sequential splitting method, the Strang splitting method has one more order of accuracy in time. Now, we analyze the stability of the splitting spectral method for the DP equations.

Proposition 4.1. *If we define the usual discrete l^2-norm on the box Ω as $\|\boldsymbol{\Psi}^n\|_{l^2}^2 = h_1\cdots h_d\sum_{\boldsymbol{p}\in\mathcal{L}}|\boldsymbol{\Psi}_{\boldsymbol{p}}^n|^2, (d=1,2,3)$, then we have*

$$\|\boldsymbol{\Psi}^{n+1}\|_{l^2}^2 = \|\boldsymbol{\Psi}^n\|_{l^2}^2, \quad n=0,1,2,\cdots. \tag{47}$$

Proof. (1) From Eqs.(36)-(40), we have

$$\begin{aligned}
&\frac{1}{h_1\cdots h_d}\|\boldsymbol{\Psi}^{n+1}\|_{l^2}^2 = \sum_{\boldsymbol{p}\in\mathcal{L}}|\boldsymbol{\Psi}_{\boldsymbol{p}}^{n+1}|^2 = \sum_{\boldsymbol{p}\in\mathcal{L}}|\sum_{\boldsymbol{j}\in\mathcal{M}}\boldsymbol{P}\,e^{\boldsymbol{\Lambda}\Delta t}\,\boldsymbol{P}^{-1}\,\hat{\boldsymbol{\Psi}}_{\boldsymbol{j}}^{**}\,e^{i\boldsymbol{\mu}_{\boldsymbol{j}}\cdot(\boldsymbol{x}_{\boldsymbol{p}}-\boldsymbol{a})}|^2\\
&= M_1\cdots M_d\sum_{\boldsymbol{j}\in\mathcal{M}}|\boldsymbol{P}\,e^{\boldsymbol{\Lambda}\Delta t}\,\boldsymbol{P}^{-1}\,\hat{\boldsymbol{\Psi}}_{\boldsymbol{j}}^{**}|^2 = M_1\cdots M_d\sum_{\boldsymbol{j}\in\mathcal{M}}|\hat{\boldsymbol{\Psi}}_{\boldsymbol{j}}^{**}|^2\\
&= \frac{1}{M_1\cdots M_d}\sum_{\boldsymbol{j}\in\mathcal{M}}|\sum_{\boldsymbol{p}\in\mathcal{L}}\boldsymbol{\Psi}_{\boldsymbol{p}}^{**}\,e^{-i\boldsymbol{\mu}_{\boldsymbol{j}}\cdot(\boldsymbol{x}_{\boldsymbol{p}}-\boldsymbol{a})}|^2 = \sum_{\boldsymbol{p}\in\mathcal{L}}|\boldsymbol{\Psi}_{\boldsymbol{p}}^{**}|^2\\
&= \sum_{\boldsymbol{p}\in\mathcal{L}}|\boldsymbol{P}_{\boldsymbol{p}}^n\,e^{-i\Delta t\boldsymbol{\Lambda}_{\boldsymbol{p}}^n}\,(\boldsymbol{P}_{\boldsymbol{p}}^n)^{-1}\,\boldsymbol{\Psi}_{\boldsymbol{p}}^*|^2 = \sum_{\boldsymbol{p}\in\mathcal{L}}|\boldsymbol{\Psi}_{\boldsymbol{p}}^*|^2\\
&= \sum_{\boldsymbol{p}\in\mathcal{L}}|e^{-i(\boldsymbol{\beta}-\phi_{\boldsymbol{p}}^{n+1}\boldsymbol{I})\Delta t}\,\boldsymbol{\Psi}_{\boldsymbol{p}}^n|^2 = \sum_{\boldsymbol{p}\in\mathcal{L}}|\boldsymbol{\Psi}_{\boldsymbol{p}}^n|^2 = \frac{1}{h_1\cdots h_d}\|\boldsymbol{\Psi}^n\|_{l^2}^2.
\end{aligned}$$

Therefore, $\|\boldsymbol{\Psi}^{n+1}\|_{l^2}^2 = \|\boldsymbol{\Psi}^n\|_{l^2}^2, \quad n=0,1,2,\cdots.$

(2) From Eqs.(42)-(46), applying the Strang splitting method in time,

$$\begin{aligned}
&\frac{1}{h_1\cdots h_d}\|\boldsymbol{\Psi}^{n+1}\|_{l^2}^2 = \sum_{\boldsymbol{p}\in\mathcal{L}}|\boldsymbol{\Psi}_{\boldsymbol{p}}^{n+1}|^2 = \sum_{\boldsymbol{p}\in\mathcal{L}}|\sum_{\boldsymbol{j}\in\mathcal{M}}\boldsymbol{P}\,e^{\boldsymbol{\Lambda}\Delta t/2}\,\boldsymbol{P}^{-1}\,\hat{\boldsymbol{\Psi}}_{\boldsymbol{j}}^{***}\,e^{i\boldsymbol{\mu}_{\boldsymbol{j}}\cdot(\boldsymbol{x}_{\boldsymbol{p}}-\boldsymbol{a})}|^2\\
&= M_1\cdots M_d\sum_{\boldsymbol{j}\in\mathcal{M}}|\boldsymbol{P}\,e^{\boldsymbol{\Lambda}\Delta t/2}\,\boldsymbol{P}^{-1}\hat{\boldsymbol{\Psi}}_{\boldsymbol{j}}^{***}|^2 = M_1\cdots M_d\sum_{\boldsymbol{j}\in\mathcal{M}}|\hat{\boldsymbol{\Psi}}_{\boldsymbol{j}}^{***}|^2\\
&= \frac{1}{M_1\cdots M_3}\sum_{\boldsymbol{j}\in\mathcal{M}}|\sum_{\boldsymbol{p}\in\mathcal{L}}\boldsymbol{\Psi}_{\boldsymbol{p}}^{***}\,e^{-i\boldsymbol{\mu}_{\boldsymbol{j}}\cdot(\boldsymbol{x}_{\boldsymbol{p}}-\boldsymbol{a})}|^2 = \sum_{\boldsymbol{p}\in\mathcal{L}}|\boldsymbol{\Psi}_{\boldsymbol{p}}^{***}|^2\\
&= \sum_{\boldsymbol{p}\in\mathcal{L}}|\boldsymbol{P}_{\boldsymbol{p}}^n\,e^{-i\Delta t\boldsymbol{\Lambda}_{\boldsymbol{p}}^n}\,(\boldsymbol{P}_{\boldsymbol{p}}^n)^{-1}\,\boldsymbol{\Psi}_{\boldsymbol{p}}^{**}|^2 = \sum_{\boldsymbol{p}\in\mathcal{L}}|\boldsymbol{\Psi}_{\boldsymbol{p}}^{**}|^2 = \sum_{\boldsymbol{p}\in\mathcal{L}}|e^{-i(\boldsymbol{\beta}-\phi_{\boldsymbol{p}}^{n+1}\boldsymbol{I})\Delta t}\,\boldsymbol{\Psi}_{\boldsymbol{p}}^*|^2\\
&= \sum_{\boldsymbol{p}\in\mathcal{L}}|\boldsymbol{\Psi}_{\boldsymbol{p}}^*|^2 = \sum_{\boldsymbol{p}\in\mathcal{L}}|\sum_{\boldsymbol{j}\in\mathcal{M}}\boldsymbol{P}\,e^{\boldsymbol{\Lambda}\Delta t/2}\,\boldsymbol{P}^{-1}\,\hat{\boldsymbol{\Psi}}_{\boldsymbol{j}}^{n}\,e^{i\boldsymbol{\mu}_{\boldsymbol{j}}\cdot(\boldsymbol{x}_{\boldsymbol{p}}-\boldsymbol{a})}|^2 = \sum_{\boldsymbol{p}\in\mathcal{L}}|\boldsymbol{\Psi}_{\boldsymbol{p}}^n|^2\\
&= \frac{1}{h_1\cdots h_d}\|\boldsymbol{\Psi}^n\|_{l^2}^2.
\end{aligned}$$

Again, we show the stability of the method with Parseval's equation [8]. □

From **Proposition** 4.1, we conclude that the new method is unconditionally stable. Next we briefly establish error estimates. Under proper assumptions of the exact solution $\boldsymbol{\Psi}(\boldsymbol{x},t)$ and electromagnetic potentials, it is easy to show the following local error estimates via the formal Lie calculus introduced in [19]:

Proposition 4.2. *For the Sequential splitting spectral method, it holds that:*

$$\|\boldsymbol{\Psi}(\boldsymbol{x},t_n) - I_{\mathcal{M}}(\boldsymbol{\Psi}^n(\boldsymbol{x}))\|_{L^2} \lesssim h^{m_0} + \Delta t^1, \quad n=0,1,2,\cdots, \tag{48}$$

where $h = max\{h_1, \cdots, h_d\}$ *and* m_0 *depends on the regularity of* $\boldsymbol{\Psi}(\boldsymbol{x}, t_0)$.

Proposition 4.3. *For the Strang splitting spectral method*

$$\|\boldsymbol{\Psi}(\boldsymbol{x}, t_n) - I_{\mathcal{M}}(\boldsymbol{\Psi}^n(\boldsymbol{x}))\|_{L^2} \lesssim h^{m_1} + \Delta t^2, \quad n = 0, 1, 2, \cdots, \tag{49}$$

where $h = max\{h_1, \cdots, h_d\}$, *and* m_1 *also depends on the regularity of* $\boldsymbol{\Psi}(\boldsymbol{x}, t_0)$.

We omit the details of proof here. One may find some hints from [3].

5. Numerical results

In this section, we first test numerical accuracy for the Sequential splitting and Strang splitting Fourier spectral method for the nonlinear Dirac equations in one dimension, respectively. Next, we apply the proposed splitting spectral method to solve the DP equations in 1-d, 2-d and 3-d, respectively.

In nonlinear Dirac equations, we define the following error function to quantify the numerical method,

$$E_{\Psi_l}(t) = \|\Psi_l^{exact}(\cdot, t) - \Psi_l^{h_1, \Delta t}(\cdot, t)\|_\infty, \quad l = 1, 2,$$

where $\Psi_l^{exact}(\cdot, t)$ denotes the exact solution of the equation, $\Psi_l^{h_1, \Delta t}$ is the numerical solution with mesh size h_1 and time step Δt.

In Dirac-Poisson equations, we can make Ψ_l, ϕ be the 'exact' solutions which are obtained numerically via using our numerical method with a very fine mesh and time step (e.g. $h_1 = 1/64, \Delta t$ =1e-03 in one dimension, $h_1 = h_2 = 1/32, \Delta t$ =1e-03 in two dimension and $h_1 = h_2 = h_3 = 1/8, \Delta t$ =1e-03 in three dimension), and $\Psi_l^{\boldsymbol{h}, \Delta t}, \phi^{\boldsymbol{h}, \Delta t}$ be the numerical solution with mesh size $\boldsymbol{h}$ and time time step Δt. To quantify the numerical method, we define the error functions as

$$E_{\Psi_l}(t) = \|\Psi_l(\cdot, t) - \Psi_l^{\boldsymbol{h}, \Delta t}(\cdot, t)\|_\infty,\ l = 1, 2, 3, 4,\ E_\phi(t) = \|\phi(\cdot, t) - \phi^{\boldsymbol{h}, \Delta t}(\cdot, t)\|_\infty.$$

5.1. Numerical tests for 1d nonlinear Dirac equations. In this section, we consider the following nonlinear Dirac equations in one dimension [15]

$$\begin{gathered} \partial_t \boldsymbol{\Psi} = \boldsymbol{A}\partial_1 \boldsymbol{\Psi} + if(|\Psi_1|^2 - |\Psi_2|^2)\boldsymbol{B}\boldsymbol{\Psi}, \quad x_1 \in \Omega, \quad t \geq 0, \\ \boldsymbol{\Psi}(a_1, t) = \boldsymbol{\Psi}(b_1, t), \quad t \geq 0 \\ \boldsymbol{\Psi}(x_1, 0) = \boldsymbol{\Psi}_0(x_1), \quad x_1 \in \Omega. \end{gathered}$$

where $\boldsymbol{\Psi}(x_1, t) = (\Psi_1(x_1, t), \Psi_2(x_1, t))^T, f(s) = m - 2\lambda s (m, \lambda \in \mathbb{R})$, $\boldsymbol{A}$ and $\boldsymbol{B}$ denote the matrices

$$\boldsymbol{A} = \begin{pmatrix} 0 & -1 \\ -1 & 0 \end{pmatrix}, \quad \boldsymbol{B} = \begin{pmatrix} -1 & 0 \\ 0 & -1 \end{pmatrix}.$$

When $m = 1, \lambda = 1/2$, one of the solitary wave solutions to the nonlinear Dirac equations is

$$\begin{aligned} \Psi_1^{exact}(x_1, t) =& \Big(\frac{\sqrt{(\gamma+1)(1-\Lambda^2)(1+\Lambda)}cosh(\sqrt{1-\Lambda^2}\tilde{x}_1)}{1+\Lambda cosh(2\sqrt{1-\Lambda^2}\tilde{x}_1)} \\ &+ sign(\nu)\frac{i\sqrt{(\gamma-1)(1-\Lambda^2)(1-\Lambda)}sinh(\sqrt{1-\Lambda^2}\tilde{x}_1)}{1+\Lambda cosh(2\sqrt{1-\Lambda^2}\tilde{x}_1)}\Big)e^{-i\Lambda\tilde{t}}, \\ \Psi_2^{exact}(x_1, t) =& \Big(\frac{i\sqrt{(\gamma+1)(1-\Lambda^2)(1-\Lambda)}sinh(\sqrt{1-\Lambda^2}\tilde{x}_1)}{1+\Lambda cosh(2\sqrt{1-\Lambda^2}\tilde{x}_1)} \\ &+ sign(\nu)\frac{\sqrt{(\gamma-1)(1-\Lambda^2)(1+\Lambda)}cosh(\sqrt{1-\Lambda^2}\tilde{x}_1)}{1+\Lambda cosh(2\sqrt{1-\Lambda^2}\tilde{x}_1)}\Big)e^{-i\Lambda\tilde{t}}, \end{aligned}$$

with $\Lambda = 0.75, \gamma = \frac{1}{\sqrt{1-\nu^2}}, \tilde{x}_1 = \gamma(x_1 - \nu t)$ and $\tilde{t} = \gamma(t - \nu x_1)$.

TABLE 1. Spatial error analysis for the two splitting spectral methods in solving 1-d Dirac equations.

M_1		32	64	128	256
Sequential splitting	$E_{\Psi_1}(t)$	3.1891e-03	2.7039e-05	8.8319e-07	8.8443e-07
	$E_{\Psi_2}(t)$	4.1022e-04	2.5791e-05	1.5073e-06	1.5179e-06
	CPU time(s)	0.059901	0.086839	0.170166	0.299854
Strang splitting	$E_{\Psi_1}(t)$	3.1890e-03	2.6706e-05	1.0127e-07	8.1613e-08
	$E_{\Psi_2}(t)$	4.1052e-04	2.5513e-05	4.8552e-08	5.4227e-08
	CPU time(s)	0.883664	1.649848	3.199256	6.180290

TABLE 2. Temporal error analysis for the two splitting spectral method in solving 1-d Dirac equations.

Δt		0.1	0.05	0.025	0.0125
Sequential splitting	$E_{\Psi_1}(t)$	8.7993e-04	4.4126e-04	2.2089e-04	1.1050e-04
	$E_{\Psi_2}(t)$	1.5079e-03	7.5405e-04	3.7707e-04	1.8854e-04
	CPU time(s)	0.008800	0.015298	0.011713	0.016307
Strang splitting	$E_{\Psi_1}(t)$	1.6536e-05	4.1355e-06	1.0382e-06	2.6407e-07
	$E_{\Psi_2}(t)$	4.2901e-05	1.0719e-05	2.6806e-06	6.7152e-07
	CPU time(s)	0.020348	0.027796	0.034608	0.052385

To measure the accuracy of our method at time $t = 0.1$, we have carried out experiments for different M_1 and Δt, considering $x_1 \in [-25, 25]$. In Table 1, we have fixed Δt=1e-04, observing the errors decrease until $M_1 = 128$, when the method achieves its maximum efficiency. And compared with the conclusion in [15], it is not difficult to find that our method has spectral accuracy in space. In Table 2, the results show that the Sequential splitting method has first-order precision and Strang splitting method has second-order precision in time.

5.2. Numerical tests for the Dirac-Poisson equations. In this section, we apply the Strang splitting spectral method to solve the DP equations in 1-d, 2-d and 3-d, respectively.

Test 1. In 1-d DP equations (13)-(14), we consider the following initial condition

$$\Psi_l(x_1, 0) = \frac{5^{1/4}}{\sqrt{2}\pi^{1/4}} e^{\frac{-5x_1^2}{2} + ix_1}, x_1 \in [-8, 8],\ l = 1, 2.$$

TABLE 3. Error analysis at time $t = 1$.

		E_{Ψ_1}	E_{Ψ_2}	E_ϕ	CPU time(s)
h_1	1/4	2.0874e-07	1.8218e-07	1.2614e-09	0.153874
	1/8	6.9023e-14	7.1819e-14	1.7989e-15	0.248460
	1/16	5.5944e-14	5.2931e-14	8.3614e-16	0.467303
	1/32	3.4949e-14	3.8143e-14	5.0654e-16	0.796025
Δt	1/20	5.4395e-04	5.4354e-04	6.5702e-05	0.086898
	1/40	1.3561e-04	1.3551e-04	3.2136e-05	0.117994
	1/80	3.3726e-05	3.3700e-05	1.5391e-05	0.182901
	1/160	8.2677e-06	8.2614e-06	7.0244e-06	0.291026

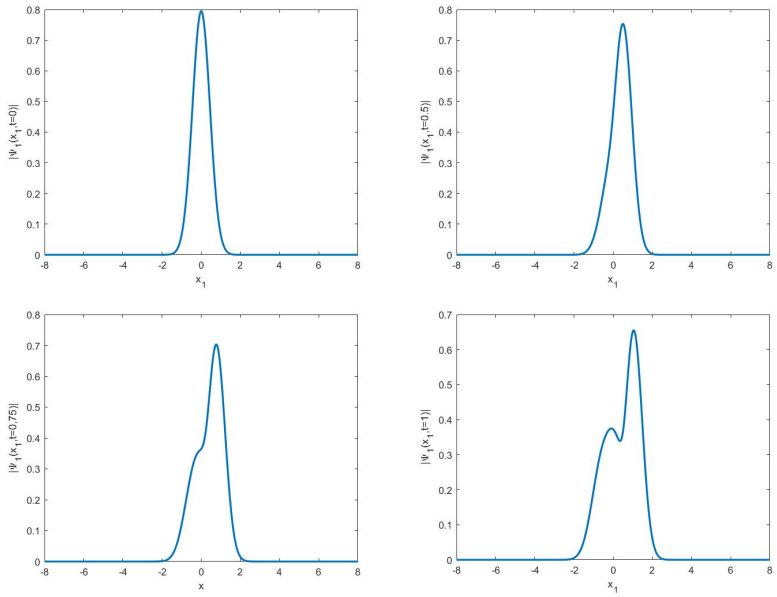

FIGURE 1. Plots for $|\Psi_1(x_1,t)|$ at t =0, 0.5, 0.75 and 1, respectively.

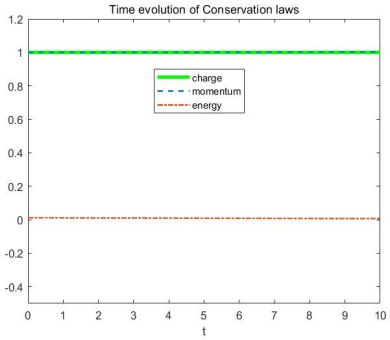

FIGURE 2. Time evolution of the charge $\mathcal{Q}(t)$, the momentum $\mathcal{P}(t)$ and the energy $\mathcal{E}(t)$.

Table 3 shows the method has spectral accuracy in space and second-order accuracy in time. Figure 1 shows us the density function $|\Psi_1(x_1,t)|$ at different times. Figure 2 shows the time evolution of the charge $\mathcal{Q}(t)$, the momentum $\mathcal{P}(t)$ and the energy $\mathcal{E}(t)$ which are presented as Eqs.(7)-(9). All of them agree with the theoretical results shown in Proposition 2.1 and the stability Proposition 4.1 in 1-d.

Test 2. In 2-d DP equations (13)-(14), we consider the following initial condition

$$\mathbf{\Psi}_l(x_1,x_2,0)=\frac{2^{1/4}}{2\sqrt{\pi}}e^{-\frac{x_1^2+x_2^2}{2}-3ix_1},\boldsymbol{x}\in[-12,12]^2,\ l=1,2,3,4.$$

TABLE 4. Error analysis at time $t = 1$.

		E_{Ψ_1}	E_{Ψ_2}	E_{Ψ_3}	E_{Ψ_4}	E_ϕ
$h_1 = h_2$	1/2	7.7745e-04	6.5441e-05	5.7766e-05	3.9590e-05	5.8118e-08
	1/4	8.3904e-13	7.8014e-13	7.7099e-13	8.1884e-13	4.9873e-16
	1/8	4.2251e-14	4.8189e-14	6.3372e-14	6.2157e-14	3.9942e-16
	1/16	4.3668e-14	4.3326e-14	5.6495e-14	5.6434e-14	4.4929e-16
Δt	1/20	2.8751e-04	3.1400e-04	3.9726e-04	2.8999e-04	1.5509e-05
	1/40	7.1636e-05	7.8270e-05	9.9020e-05	7.2312e-05	7.5601e-06
	1/80	1.7813e-05	1.9465e-05	2.4625e-05	1.7985e-05	3.6131e-05
	1/160	4.3665e-06	4.7717e-06	6.0367e-06	4.4090e-06	1.6472e-06

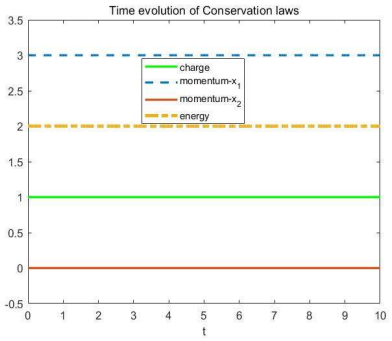

FIGURE 3. Time evolution of the charge $\mathcal{Q}(t)$, the momentum in x_1-direction, $\mathcal{P}_1(t)$, the momentum in x_2-direction, $\mathcal{P}_2(t)$ and the energy $\mathcal{E}(t)$.

Table 4 shows that the scheme has spectral accuracy in space and second-order accuracy in time. Figure 3 shows the time evolution of the charge $\mathcal{Q}(t)$, the momentum in x_1-direction, $\mathcal{P}_1(t)$, the momentum in x_2-direction, $\mathcal{P}_2(t)$ and the energy $\mathcal{E}(t)$. From this picture, we find that the proposed method keeps well the conservation laws of the DP equations in 2-d. Figure 4 shows the density function $|\Psi_1(x_1, x_2, t)|$ at different times.

Test 3. In 3-d DP equations (13)-(14), we consider the following initial condition

$$\mathbf{\Psi}_l(x_1, x_2, x_3, 0) = \frac{125^{1/4}}{2\pi^{3/4}} e^{-\frac{x_1^2+x_2^2+x_3^2}{10}+ix_1}, \boldsymbol{x} \in [-12, 12]^3,\ l = 1, 2, 3, 4.$$

TABLE 5. Error analysis at time $t = 1$.

		E_{Ψ_1}	E_{Ψ_2}	E_{Ψ_3}	E_{Ψ_4}	E_ϕ
$h_1 = h_2 = h_3$	1	2.7073e-07	1.3713e-07	2.0394e-07	8.4632e-08	1.3175e-10
	1/2	1.2010e-08	6.7110e-09	1.1227e-08	8.5682e-09	6.2113e-14
	1/4	5.9759e-09	3.1468e-09	5.5050e-09	4.0496e-09	2.5960e-15
Δt	1/20	9.4753e-05	6.7682e-05	3.9873e-05	4.9895e-05	9.5012e-07
	1/40	2.3632e-05	1.6875e-05	9.9486e-06	1.2441e-05	4.6233e-07
	1/80	5.8778e-06	4.1969e-06	2.4747e-06	3.0942e-06	2.2075e-07

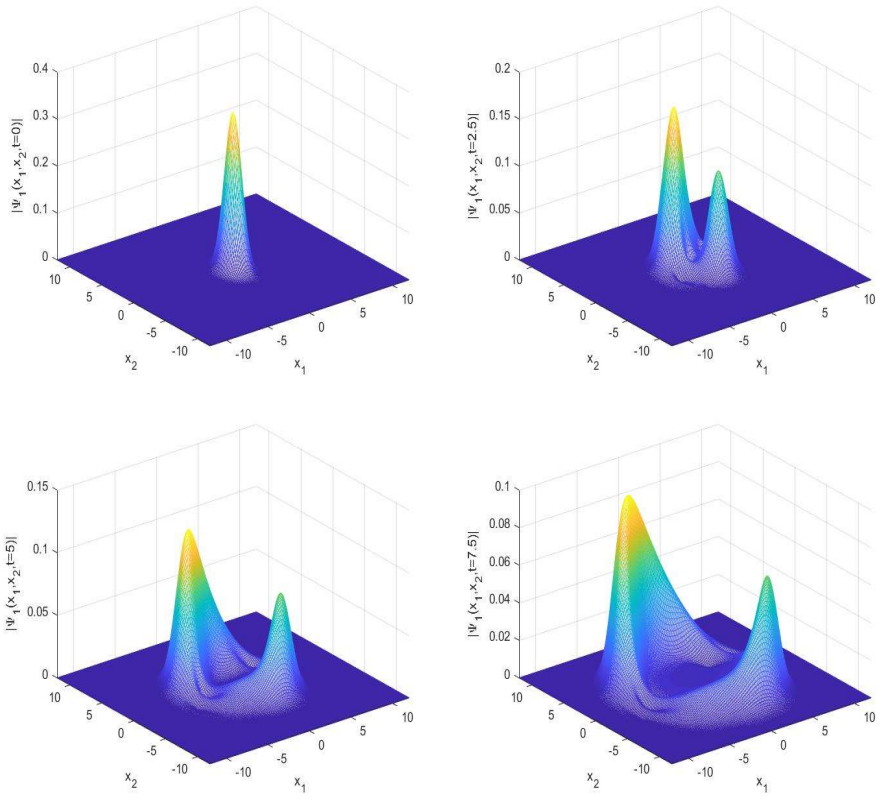

FIGURE 4. Surface plots of $|\Psi_1(x_1, x_2, t)|$ at $t = 0, 2.5, 5$ and 7.5, respectively.

FIGURE 5. Time evolution of the charge $\mathcal{Q}(t)$, the momentum in x_1-direction, $\mathcal{P}_1(t)$, the momentum in x_2-direction, $\mathcal{P}_2(t)$, the momentum in x_3-direction, $\mathcal{P}_3(t)$ and the energy $\mathcal{E}(t)$.

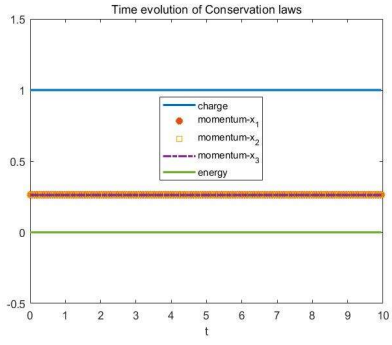

In Table 5, we find that the scheme has spectral accuracy in space and second-order accuracy in time. From Figure 5, we can also find that the splitting spectral method keeps well the conservation laws of the DP equations in 3-d, again. The density function $|\Psi_1(x_1, x_2, 0, t)|$ at different times are shown in Figure 6.

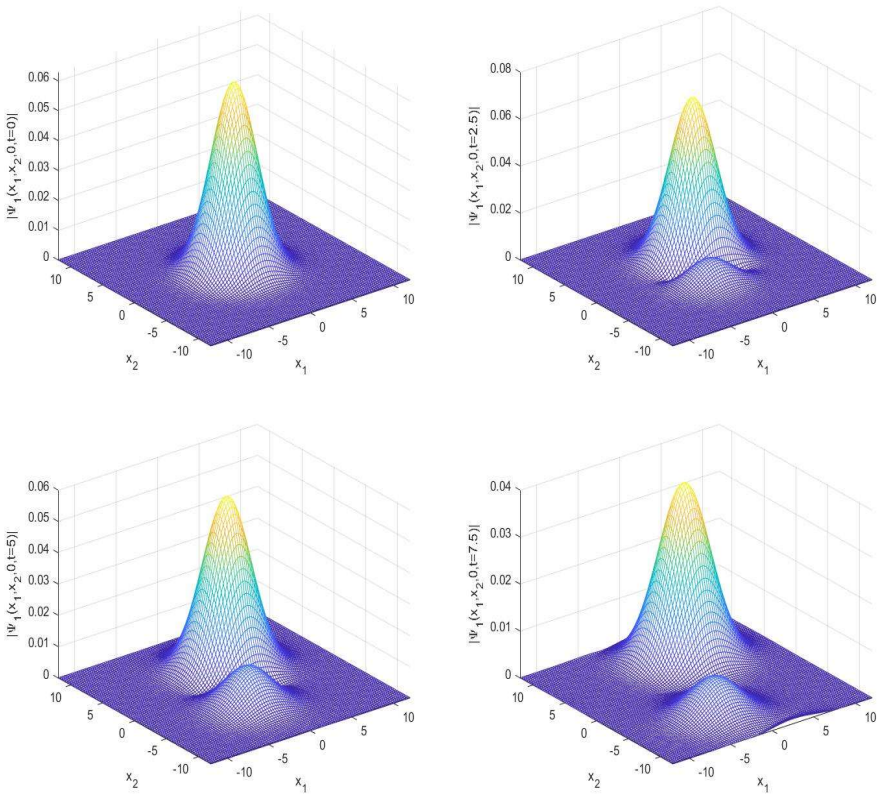

FIGURE 6. Surface plots of $|\Psi_1(x_1, x_2, 0, t)|$ at t =0, 2.5, 5 and 7.5, respectively.

5.3. A numerical application. In this subsection, we present a numerical application to investigate the spin dynamics, since the Dirac-Poisson equation presented here has automatic inclusion of electronic spin. When the external laser is assumed to be linearly polarized in the y-direction and propagates in the x-direction, the vector potential $\boldsymbol{A}$ is taken as $(0, A_y(x,t))^T$ with $A_y(x,t)$ defined as [22]

$$A_y(x,t) = \begin{cases} A_0 \frac{\omega}{\pi} t sin[\omega(t - x/c)], & 0 \le t - x/c \le \pi/\omega \\ A_0 sin[\omega(t - x/c)], & t - x/c > \pi/\omega \end{cases}$$

where A_0 is the maximum field amplitude of the laser pulse, ω is the frequency of laser and $c = 137$. The starting point for the time evolution of the atom under the influence of the external laser field is

$$\boldsymbol{\Psi}(x, y, 0) = Ne^{-2r} r^{(\epsilon-1)/2} (\sqrt{1+\epsilon}, 0, i\frac{y}{r}\sqrt{1-\epsilon}, i\frac{x}{r}\sqrt{1-\epsilon})^T,\ r = \sqrt{x^2+y^2}$$

with $\epsilon^2 = 1 - 4/137^2$. Here N is defined as the normalization constant such that $||\boldsymbol{\Psi}||^2 = 1$. In the numerical simulation presented below, the time step is given by Δt= 1e-03, the spatial domain $\Omega = [-8, 8] \times [-8, 8]$ is divided into $M_x \times M_y = 128^2$ subdomains. The effects of the magnetic field (the electron is pushed in the propagation direction of the laser pulse) with short-time evolution are showed in Figure 7. The three images in the top row show the density $|\Psi_1(x, y, t)|$ at different times for a nonrelativistic case ($A_0 = 109.6, \omega = 10$) and the bottom row shows the

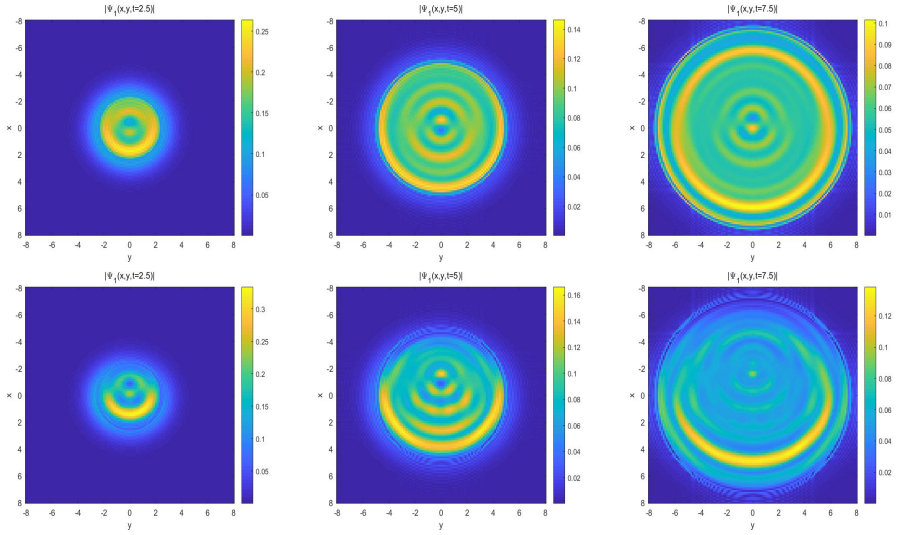

FIGURE 7. Image plots for $|\Psi_1(x, y, t)|$ at t =2.5, 5 and 7.5 for two cases. Case 1: a nonrelativistic regime ($A_0 = 109.6, \omega = 10$) in the top row; Case 2: a relativistic regime ($A_0 = 411, \omega = 10$) in the bottom row.

apparent movement of cone points when the electron is pushed in the direction of laser propagation($+x$-direction) for a relativistic case ($A_0 = 411, \omega = 10$).

In addition, Figure 8 shows the population of four-component for nonrelativistic and relativistic regimes. The sum of the density of four components keeps unity, i.e., $||\mathbf{\Psi}(x, y, t)||_{l^2}^2 = 1$. However, the decrease in the first component relative to the second one indicates spin-flip, as it can be seen on the top row of Figure 8. The same conclusion can be drawn from the bottom row of Figure 8. The top two images have the same period of perturbation as the bottom two, but the amplitude of spin-flip in the relativistic case is stronger than those in the nonrelativistic case.

6. Conclusion

We proposed a splitting spectral method for the time-dependent Dirac-Poisson equations and found that both Sequential splitting method and Strang splitting method can hold unconditionally stable numerical results. And their differences are also clear, the former has low precision and fast calculation speed, while the latter has high precision and slow calculation speed. Besides, Fourier spectral method and Sine spectral method are developed for the Dirac-Poisson equations, respectively. In the build up of the numerical algorithm, diagonalization of matrix makes the method go smoothly. Finally, the numerical tests in 1-d, 2-d and 3-d show the two splitting spectral methods both have spectral-order accuracy in space, keep the conservation laws well. Through numerical study for the 2-d DP equations with external laser field, we find some phenomena of spin-flip dynamics. In the future, combining the perfectly matched layer method, we can apply the proposed numerical method to describe more complicated phenomena of quantum electrodynamics.

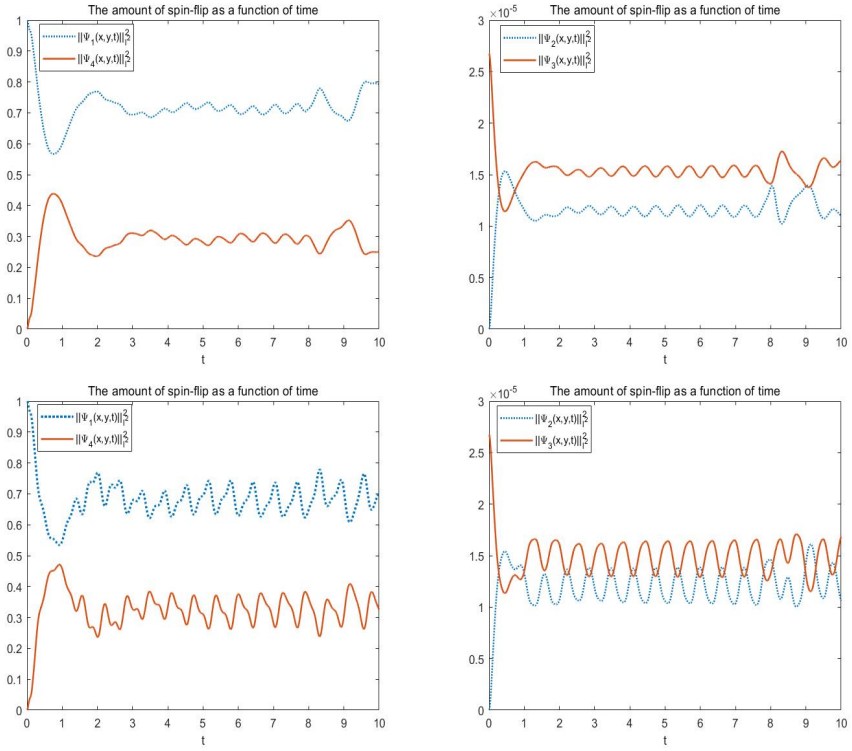

FIGURE 8. Image plots for the spin-flip for two regimes. Case 1: a nonrelativistic regime ($A_0 = 109.6, \omega = 10$) in the top row; Case 2: a relativistic regime ($A_0 = 411, \omega = 10$) in the bottom row.

Acknowledgments

The research of H. Wang is supported in part by the Natural Science Foundation of China (NSFC) under grant Nos. 11871418 and 11971120, by Yunnan Fundamental Research Projects under grant No. 202101AS070044, and by Program for Innovative Research Team on Science and Technology in Universities of Yunnan Province. And the research of Y. Zhang is supported by the Natural Science Foundation of China (NSFC) under grant No. 12271400.

References

[1] X. Antoine, F. Fillion-Gourdeau, E. Lorin, S. MacLean, Pseudospectral computational methods for the time-dependent Dirac equation in static curved spaces. Journal of Computational Physics. 411 (2020) 1-23.

[2] W. Bao, Y. Cai, Mathematical theory and numerical methods for Bose-Einstein condensation. Kinetic and Related Models. 6 (2013) 1-135.

[3] W. Bao, Y. Cai, X. Jia, et al, Error estimates of numerical methods for the nonlinear Dirac equation in the nonrelativistic limit regime. Science China Mathematics. 59(8)(2016) 1461-1494.

[4] W. Bao, X. Li, An efficient and stable numerical method for the Maxwell-Dirac system. Journal of Computational Physics. 199(2)(2004) 663-687.

[5] M.A. Botchev, I. Faragó, R. Horváth, Application of operator splitting to the Maxwell equations including a source term. Applied Numerical Mathematics. 59 (2009) 522-541.

[6] N. Bournaveas, G.E. Zouraris, Split-step spectral scheme for nonlinear Dirac systems. ESAIM: Mathematical Modelling and Numerical Analysis. 46 (2012) 841-874.

[7] D. Brinkman, C. Heitzinger, P.A. Markowich, A convergent 2D finite-difference scheme for the Dirac-Poisson system and the simulation of graphene. Journal of Computational Physics. 257 (2014) 318-332.
[8] C. Canuto, A. Quarteroni, M.Y. Hussaini, T.A. Zang, Spectral Methods. Springer-Verlag Berlin Heidelberg (2007).
[9] J.M. Chadam, R.T. Glassey, On the Maxwell-Dirac equations with zero magnetic field and their solution in two space dimensions. Journal of mathematical analysis and applications. 53(3)(1976) 495-507.
[10] Y.H. Ding, T. Xu, On semi-classical limits of ground states of a nonlinear Maxwell-Dirac system. Calculus of Variations and Partial Differential Equations. 51 (2014) 17-44.
[11] L. Einkemmer, A. Ostermann, Convergence analysis of a discontinuous Galerkin/Strang splitting approximation for the Valsov-Poisson equations. Society for Industrial and Applied Mathematics. 52(2)(2014) 757-778.
[12] M.J. Esteban, M. Lewin, E. Séré, Variational methods in relativistic quantum mechanics. Bulletin (New Series) of the American Mathematical Society. 45 (2008) 535-593.
[13] M.J. Esteban, E. Sere, Existence de solutions stationnaires pour l'équation de Dirac non linéaire et le système de Dirac-Poisson. Comptes rendus de l'Académie des sciences. Série 1. Mathematics. 319(11)(1994) 1213-1218.
[14] I. Faragó, Á. Havasi, On the convergence and local splitting error of different splitting schemes. Progress in Computational Fluid Dynamics. 5(8)(2005) 495-504.
[15] F. Hoz, F. Vadillo, An integrating factor for nonlinear Dirac equations. Computer Physics Communications. 181(7)(2010) 1195-1203.
[16] Z.Y. Huang, S. Jin, P.A. Markowich, C. Sparber, C.X. Zheng, A time-splitting spectral scheme for the Maxwell-Dirac system. Journal of Computational Physics. 208(2)(2005) 761-789.
[17] X.G. Li, C.K. Chan, Y. Hou, A numerical method with particle conservation for the Maxwell-Dirac system. Applied Mathematics and Computation. 216 (2010) 1096-1108.
[18] A.G. Lisi, A solitary wave solution of the Maxwell-Dirac equations. Journal of Physics A: Mathematical and General. 28(18)(1995) 5385-5392.
[19] C. Lubich, On splitting methods for Schrödinger-Poisson and cubic nonlinear Schrödinger equations. Mathematics of computation. 77 (2008) 2141-2153.
[20] J.C. Maxwell, A dynamical theory of the electromagnetic field. The Royal Society of London (1865).
[21] J.C. Maxwell, A treatise on electricity and magnetism. Nature (1873).
[22] U.W. Rathe, C.H. Keitel, M. Protopapas and P.L. Knight, Intense laser-atom dynamics with the two-dimensional Dirac equation. Journal of Physics B: Atomic, Molecular and Optical Physics. 30(15)(1997) L531-L539.
[23] B. Saha, Nonlinear spinor fields and its role in cosmology. International Journal of Theoretical Physics. 51 (2012) 1812-1837.
[24] K. Schratz, Y. Wang, X. Zhao, Low-regularity integrators for nonlinear Dirac equations. Mathematics of Computation. 90 (2021) 189-214.
[25] S.H. Shao, H.Z. Tang, Higher-order accurate Runge-Kutta discontinuous Galerkin methods for a nonlinear Dirac model. Discrete Continuous Dynamical Systems-B. 6(3)(2006) 623-640.
[26] B. Thaller, The Dirac Equation. Springer, Berlin (1992).
[27] M. Wakano, Intensely localized solutions of the classical Dirac-Maxwell field equations. Progress of Theoretical Physics. 35(6)(1966) 1117-1141.
[28] H.Q. Wang, Z.G. Liang, R.H. Liu, A splitting Chebyshev collocation method for Schrödinger-Poisson system. Computational and Applied Mathematics. 37 (2018) 5034-5057.
[29] H. Wang, H.Z. Tang, An efficient adaptive mesh redistribution method for a nonlinear Dirac equation. Journal of Computational Physics. 222(1)(2007) 176-193.
[30] J. Xu, S.H. Shao, H.Z. Tang, Numerical methods for nonlinear Dirac equation. Journal of Computational Physics. 245(2013) 131-149.
[31] J. Zhang, W. Zhang, X. Tang, Existence and multiplicity of solution for nonlinear Dirac-Poisson systems. Electronic Journal of Differential Equations. 91 (2017) 1-17.

College of Mathematics, Sichuan University, Chengdu 610065, China
E-mail: wangdandan@stu.scu.edu.cn

Center for Applied Mathematics, Tianjin University, Tianjin 300072, China
E-mail: Zhang_Yong@tju.edu.cn

School of Statistics and Mathematics, Yunnan University of Finance and Economics, Kunming 650221, China; School of Mathematics, Yunnan Normal University, Kunming 650500, China.
E-mail: hanquan.wang@gmail.com